Protein Folding in Classical Perspective: Folding of Horse Cytochrome *c*[†]

Abani K. Bhuyan,* D. Krishna Rao, and N. Prakash Prabhu

School of Chemistry, University of Hyderabad, Hyderabad 500046, India

Received September 27, 2004; Revised Manuscript Received November 21, 2004

ABSTRACT: Proteins meet with the stipulations of Levinthal. Two test tube variants of ferrocytochrome *c* (ferrocyt *c*) whose thermodynamic stabilities are vastly different refold to the same global minimum under a given final native condition, and they do so quickly at rates that do not reflect a strong dependence on the thermodynamic driving force. The transition-state ensemble is more unfolded-like, and the folding barrier offered is energetically sizable. The experiments involve neutral- (pH 7) and alkaline ferrocyt *c* pH (12.7), whose aqueous stabilities are 18 (±0.3) and 3 (±0.5) kcal mol^{-1}, respectively. But the large disparity in thermodynamic stability is not strongly reflected in their refolding rates. Cross-pH studies, where GdnHCl-unfolded states of neutral- and alkaline ferrocyt *c* are allowed to refold to the same final pH and denaturant concentration, indicate that the refolding rates are largely independent of the stability, configuration, ionization, and solvation of the initial unfolded state. Also, burst relaxation signals in cross-pH refolding runs show the same quantitative dependence on GdnHCl, suggesting that the earliest relaxation or reconfiguration of the chains must be the same and is independent of the initial equilibrium unfolded state. Analyses along the classical line indicate an early transition state where much less than a third of the protein surface that is buried in the native state becomes buried. The barrier energy is of the order of 10 k_BT. The results, apparently inconsistent with the predictions of the funnel model, afford a mechanistic description of folding in which the folding time of small single-domain proteins is set by the time needed for the denatured polypeptide to search-find a nativelike topology.

While the finding of sequential involvement of kinetic intermediates for a sizable set of proteins (*1*, *2*) appears to provide clues to the Levinthal enigma, observations of apparently two-state fast folding, where intermediates do not accumulate (*3*−*8*), raises doubts that the engagement of kinetic intermediates resolves the conformational search problem. Reports of misfold organization of a kinetic intermediate of ferricytochrome *c* (ferricyt *c*)[1] also raised the question of how conducive intermediates are to folding (*9*, *10*).

Emerging ideas of landscape perspective or the funnel model (*11*−*16*) were first used to interpret both two-state folding kinetics and accumulation of misfolded structures on the basis of size, slope, and roughness of energy landscapes (*17*, *18*). Corroboration between experimental and simulation results has also been shown regarding the fractional φ values for CI2 (*19*). The landscape view holds that the funneled organization of the energy landscape dominates the folding kinetics because the great variety of detailed mechanisms existing on the funnel influences the folding trajectories (*16*). The emerging ideas, however, often appear to undermine some of the strongly established empirical patterns of folding kinetics. These patterns, including the energy and the location of the folding barrier, which form the key elements of the classical view of folding, are not reproduced in the new paradigm. Overlooking empirical results is difficult. A number of recent studies have demonstrated the involvement of sequential intermediates in the folding pathway of cyt *c* (*20*−*23*). It has also been shown that the misfold organization of the folding intermediate is associated with an optional event, and it does not negate the classical description of folding (*10*). Application of the classical paradigm to a number of proteins exhibiting diverse folding behavior has been discussed (*24*).

Supported by empirical observations on ferrocytochrome *c* (ferrocyt *c*), this paper presents arguments to show the self-sufficiency of the classical perspective toward a mechanistic description of folding of small proteins. Ferrocyt *c* is intrinsically a two-state "fast folder" (*8*, *25*, *26*). The neutral and alkaline pH forms of the protein, which are greatly different in thermodynamic stability, have been used to demonstrate that folding is under thermodynamic control and that an initial search regime limits the folding speed. Biologically relevant folding time of small two-state proteins can be approximately equated to the time needed for the nascent polypeptide to find a stable but less nativelike rate-limiting barrier.

MATERIALS AND METHODS

Cyt *c* was from Sigma (Type VI). GdnHCl and sodium dithionite were obtained from USB and Merck, respectively. Experiments were done in strictly anaerobic atmosphere at 22 °C using 0.1 M sodium phosphate buffer for pH 7

[†] This work was supported by grants from Department of Biotechnology (BRB/15/227/2001), Department of Science and Technology (4/1/2003-SF), and University Grants Commission (UPE Funding), Government of India.

* To whom correspondence should be addressed. E-mail: akbsc@uohyd.ernet.in. Fax: 91-40-23012460.

[1] Abbreviations: GdnHCl, guanidine hydrochloride; cyt *c*, cytochrome *c*; ferricyt *c*, ferricytochrome *c*; ferrocyt *c*, ferrocytochrome *c*.

10.1021/bi047897n CCC: $30.25
Published on Web 02/01/2005

conditions, and NaOH or NaOD (with or without 1 mM CAPS) for pH 12.7 conditions. Solutions contained 0.5−3 mM freshly prepared sodium dithionite, and experiments were completed within 2 h of exposing the protein to high pH.

High-pH fluorescence changes were corrected by using NATA fluorescence.

NMR Spectra. D_2O solutions of 1 mM cyt *c*, the amides of which were preexchanged, were adjusted to pH 7 (0.1 M phosphate) or pH 12.7 using NaOD. Unfolded protein was prepared in GdnDCl. For reduction solid sodium dithionite was added under nitrogen to obtain a final concentration of 20 mM. The tubes were sealed with sleeved rubber stoppers. Spectra were taken at 22 °C in a 400 MHz Bruker spectrometer (AV400).

Equilibrium Unfolding. Cyt *c* solutions were deaerated and reduced under nitrogen with ∼2 mM sodium dithionite and incubated in tightly capped quartz cuvettes or rubber-capped small glass tubes for ∼30 min. Tryptophan fluorescence emission spectra (ex: 280 nm) were taken in a FluoroMax-3 instrument (Jobin-Yvon, Horiba). Optical absorption spectra were recorded in a Cary 100 (Varian) spectrophotometer. Data were analyzed using the standard two-state equations.

Folding−Unfolding Kinetics. The general procedure for kinetic experiments under controlled anaerobic conditions has been described earlier (*8*, *25*, *26*). The protein initially unfolded in ∼7 M GdnHCl, pH 7 (or ∼5 M GdnHCl, pH 12.7) was reduced under nitrogen by adding a concentrated solution of sodium dithionite to a final concentration of ∼3 mM. The final protein concentration in the refolding mixture was 44 μM when both initial and final conditions of the reaction involved pH 7. Final protein concentration in cases in which either the initial or the final or both conditions involved pH 12.7 was in the 10−15 μM range. Unfolding experiments were performed following the same procedure of two-syringe mixing. The final protein concentration in unfolding experiments within pH 7 was ∼28 μM, but was reduced to 6−10 μM range whenever the condition of pH 12.7 was engaged. Fluorescence-probed kinetics were measured at 22 °C using a SFM 400 mixing module (Biologic). Excitation wavelength was 280 nm, and emission was measured using a 335 nm cutoff filter. Typically, 10−20 shots were averaged.

Kinetic traces were analyzed using single- or double-exponential functions to extract apparent rates, λ_i, the initial signal, S_o, which corresponds to the "zero-time" signal in the stopped-flow time window, the observed signal, S_{obs}, and the final equilibrium signal, S_∞, corresponding to the signal value at $t = t_\infty$. The S_o, S_{obs}, and S_∞ signals were subjected to initial normalization by first subtracting the buffer fluorescence signals, and then dividing by the recorded signal of the unfolded protein in the highest GdnHCl concentration. In the unfolding set of measurements the S_∞ value of the kinetic trace at the highest concentration of GdnHCl employed was used to divide the fluorescence signals. To account for curvatures at extremities of folding and unfolding limbs rate-denaturant data were fitted using quadratic equations (*27*). The fitted values of k_f° and k_u° were compared with those calculated by the use of the equation: $\log k_f^\circ = \log k_u^\circ - \log K^\circ$.

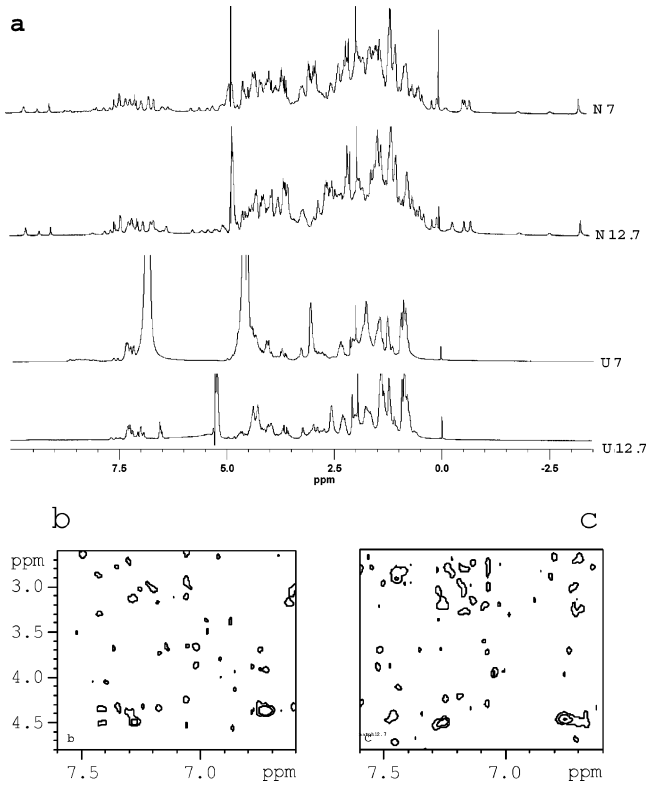

FIGURE 1: 400 MHz NMR spectra of ferrocytochrome *c*. (a) Native states at pH 7 (N7) and pH 12.7 (N12.7), and GdnDCl-unfolded states at pH 7 (U7) and pH 12.7 (U12.7). (b and c) Regions of native-state NOESY spectra of neutral and alkaline ferrocytochrome *c*.

RESULTS

Neutral and Alkaline Forms of Ferrocyt c. Ferrocyt *c* at pH 12.7 (alkaline ferrocyt *c*) is substantially structured. The NMR spectrum in Figure 1a shows chemical shift dispersion characteristic of a secondary- and tertiary-structured protein. Minor changes in both intensities and chemical shifts of resonances, relative to those seen for the native protein at pH 7 (neutral ferrocyt *c*), indicate some readjustments of side chains. The spectrum does not hint at molecular aggregation. In fact, TOF mass spectra and extensive ligand-binding experiments (data not shown) indicate no deamidation or aggregation at alkaline pH. A large number of NOE peaks seen at neutral pH appear at alkaline pH also, albeit somewhat shifted (Figure 1b,c). Figure 1a also compares the GdnDCl-unfolded NMR spectra of neutral- and alkaline ferrocyt *c*. Chemical shift dispersion is lost in both, but differences between the two are apparent, indicating differences in unfolded chain configuration. The latter also shows base-catalyzed fast exchange of residual hydrogens of GdnDCl with residual water. The resonances of guanidine and water protons coalesce as the exchange rate approaches the difference of the two chemical shifts.

Visible optical and fluorescence spectra of native and guanidine-unfolded states of ferrocyt *c* at neutral and alkaline pH were also examined (data not shown). Briefly, native-state Soret spectra of neutral and alkaline forms are not very different, but the unfolded-state spectra are. The spectra indicate that in contrast to the presence of a small population of pentacoordinate heme in guanidine-unfolded neutral ferrocyt *c* (*8*), the unfolded population at alkaline pH is

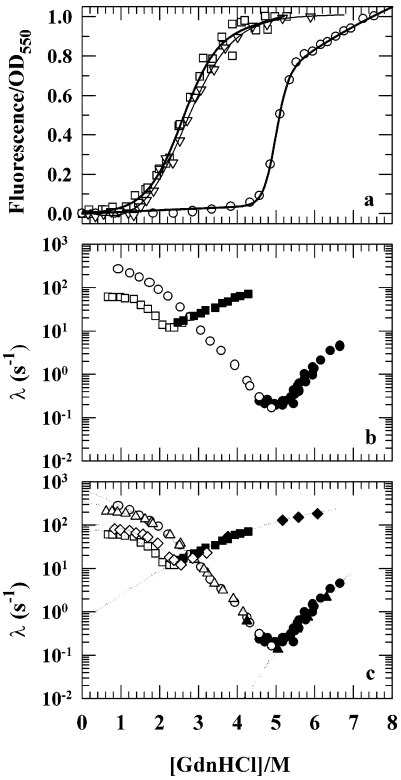

FIGURE 2: (a) GdnHCl unfolding of ferrocytochrome *c* at pH 7 (○), and pH 12.7 (□, fluorescence and ▽, optical absorption at 550 nm). Fitted values of $\Delta G(H_2O)$ and C_m are given in Table 1. (b) GdnHCl dependence of rates for the pH 7 ⇋ pH 7 (○, folding and ●, unfolding) and pH 12.7 ⇋ pH 12.7 (□, folding and ■, unfolding) equilibria. (c) Rate-denaturant dependences for all the reactions studied: pH 7 ⇋ pH 7 and pH 12.7 ⇋ pH 12.7 as in panel (b), pH 12.7 → 7 refolding (△), pH 12.7 → 7 unfolding (▲), pH 7 → 12.7 refolding (◇), and pH 7 → 12.7 unfolding (◆). Thin dotted lines are fits to data according to $\log k = \log k(H_2O) + m_1x + m_2x^2$, where x is GdnHCl concentration.

entirely hexacoordinate. In both neutral and alkaline media, the native state is fluorescence-silent, but the unfolded state is fluorescent. However, the fluorescence of unfolded alkaline ferrocyt *c* is largely quenched relative to that of the neutral-pH form, due likely to ionization of the W59 side chain. Since the intrinsic fluorescence of tryptophan is likely affected strongly at alkaline pH, it is impossible to say if the increased quenching of W59 is of any structural significance.

Stability of Neutral and Alkaline Ferrocyt c. Figure 2a compares GdnHCl unfolding transitions of the two forms. Two-state analysis of data yields a ΔG_D° value of 18 (±0.3) kcal mol^{-1} for neutral ferrocyt *c*. For the alkaline protein, ΔG_D° values obtained from fluorescence and absorbance detected transitions are 3.5 and 2.5 kcal mol^{-1}, respectively. The value reported is the average, 3 (±0.5) kcal mol^{-1} (see Table 1). Such a large difference in ΔG_D° for the neutral and alkaline ferrocyt *c* indicates drastic reduction of aqueous stability of the latter. The equilibrium *m*-values, m_g, for the neutral and alkaline forms are 3.6 (±0.1) and 1.2 (±0.1) kcal mol^{-1} M^{-1}, respectively. Since the native-state NMR spectra indicate that significant portions of secondary and tertiary structures are similar in neutral and alkaline ferrocyt *c*, the observed disparity in the m_g value is likely due to relatively small solvent accessible surface area in the denatured state of the alkaline form. The solvation free energy of the denatured chain ($= \gamma A_D$, where γ is the free energy per unit surface, and A_D refers to the solvent accessible surface area) should then be higher at neutral pH relative to that at alkaline pH (see Discussion).

Folding and Unfolding Kinetics. In general, kinetic traces were fitted to 1-exponential. In some cases 2-exponentials were needed to improve the overall quality of fits. The slow minor phase, the amplitude of which averages to ~10% of the observed signal, represents most likely the fraction of the oxidized protein. Figure 2b shows denaturant dependences of the logarithm of the fast refolding (unfolding) phase for the two proteins. In each case, the relaxation minimum closely matches the midpoint of the individual equilibrium unfolding transition (Figure 2a). Under strongly refolding and unfolding conditions, the rates deviate away from linearity. This feature of folding chevron has been described in earlier studies of ferrocyt *c* conducted at 10 °C (*8*, *25*) and is considered in much detail in the preceding article in this issue (*26*). The refolding speed at pH 12.7 appears somewhat slower relative to that at pH 7 (see below).

To examine how the structure, stability, and the configuration of the initial unfolded state affect kinetics of folding and unfolding, stopped-flow rates were measured by crossing from one pH to the other (i.e, pH 7 → 12.7 and pH 12.7 → 7) where the final condition was varied by adding different concentrations of GdnHCl. Figure 2c presents these data. For clear comparison, the individual intra-pH data sets for neutral and alkaline ferrocyt *c* (Figure 2b) have been replotted. Remarkably, the GdnHCl dependences of folding−unfolding rates are almost identical for the pH 7 → 7 and pH 12.7 → 7 refolding, except for a small difference under strongly refolding conditions (<1 M GdnHCl) where the pH 12.7 → 7 refolding rate appears to slow marginally. Likewise, denaturant dependences of folding rates measured by pH 12.7 → 12.7 and pH 7 → 12.7 refolding jumps are very similar. Folding and unfolding rates in water (k_f° and k_u°, respectively) were extracted by fitting the data to the

Table 1: Kinetic and Thermodynamic Parameters for Folding and Unfolding of Neutral and Alkaline Ferrocytochrome *c*

			$\Delta G(H_2O)$ (kcal mol^{-1})		C_m (M GdnHCl)			
	log k_f (H_2O)	log k_u (H_2O)	kinetic	equilibrium	kinetic	equilibrium	E_a^f (kcal mol^{-1})	$\alpha_f^\ddagger$
folding−unfolding								
pH 7 ⇋ pH 7	2.80	−10.5	17.8	18 (±0.3)	5.0	5.0 (±0.1)	6.95	0.10
pH 12.7 ⇋ pH 12.7	1.83	−0.27	2.8	3 (±0.5)	2.3	2.6 (±0.2)	8.2	0.21
cross-pH refolding								
pH 12.7 → pH 7	2.53						7.3	0.05
pH 7 → pH 12.7	1.95						8.1	0.29
cross-pH unfolding								
pH 12.7 → pH 7		−10.5						
pH 7 → pH 12.7		−0.24						

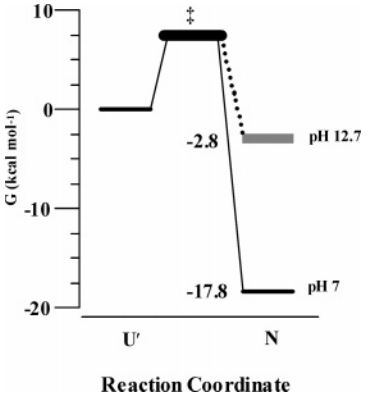

FIGURE 3: Energy level diagram for native and unfolded states, and the transition state for the refolding of neutral and alkaline ferrocyt *c*. Energy levels were calculated from kinetic data alone (Table 1), and are scaled with reference to the energy of the U′ state arbitrarily set to zero.

quadratic relationship (*26*; eq 3 in the preceding article in this issue). Aqueous stabilities of neutral and alkaline ferrocyt *c* calculated from the fitted k_f° and k_u° values are in excellent agreement with those obtained from equilibrium unfolding (Table 1).

Free Energies of the Folding Transition States, Folded States, and Unfolded States. Free energies of transition states for folding were estimated by assuming the applicability of the general thermally activated rate law: $E_a^f = -RT \ln(k/A_o)$, where k is the rate coefficient (k_f° and k_u°), and A_o is the front factor. Taking the most recent suggestion of $A_o = 1 \times 10^8$ s^{-1} (*28*), values of E_a^f calculated for neutral and alkaline ferrocyt *c* are listed in Table 1.

Figure 3 depicts free energies of the folded, unfolded, and transition states for the folding−unfolding reactions studied. It is clear that the folding energy barrier for neutral and alkaline ferrocyt *c* has the same height, even though the aqueous stabilities of the two proteins are disparate to the extent of ∼15 kcal mol^{-1}. Further, the refolding barrier size for the pH 7 → 7 and pH 12.7 → 7 refolding reactions is nearly the same (Table 1). Similarly, the value of E_a^f for pH 7 → 12.7 and pH 12.7 → 12.7 refolding reactions is comparable. These results indicate that the refolding rates and transition-state barrier heights are independent of both configuration and stability of the initial unfolded state. The extrapolated refolding rate at pH 12.7 is ∼6 (±2) fold smaller than that at pH 7 (Figure 2b,c). This may arise partly from the marginally higher value of E_a^f (∼1.2 kcal mol^{-1}) at pH 12.7 (Table 1). However, in view of the extraordinary stability difference between the neutral and alkaline forms of the protein (∼15 kcal mol^{-1}), the observed difference in the folding rate is considered insubstantial.

Location of the Transition-State Barrier. A rough estimate of the structural resemblance of the transition state to the native state is obtained from the relation, $\alpha = m^{\ddagger}_{f(u)}/m_g$, where $m_f^{\ddagger}$ and $m_u^{\ddagger}$ are, respectively, kinetic *m*-values ($= 2.3RT\,\partial \log k_{f(u)}/\partial[\text{GdnHCl}]$) for refolding and unfolding. For a nonlinear folding chevron the α-value will obviously vary with denaturant concentration. Of relevance is the value of α under strongly nativelike conditions. Table 1 lists the α-values approximated from the extrapolated k_f values for GdnHCl concentrations <0.5 M (Figure 2c). Under strongly refolding conditions (<0.5 M GdnHCl) the α-value for all refolding reactions is <0.3, suggesting that less than one-third of the protein surface that is buried in the native state becomes buried in the folding transition state. Thus, in all cases the folding transition state bears less structural resemblance to the native state.

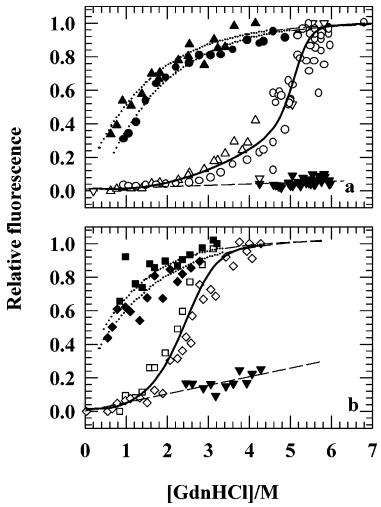

FIGURE 4: Normalized signal values at time $t = 0$ and $t = \infty$ (S_o and S_∞, respectively) in folding and unfolding kinetics. (a) S_o from pH 7 ⇋ pH 7 refolding (●) and unfolding (▼), S_o from pH 12.7 → 7 refolding (▲), S_∞ from pH 7 ⇋ pH 7 refolding and unfolding (○), and S_∞ from pH 12.7 → 7 refolding (△) and unfolding (▽) reactions. (b) S_o from pH 12.7 ⇋ pH 12.7 refolding (◆) and unfolding (▼), S_o from pH 7 → 12.7 refolding (■), S_∞ from pH 12.7 ⇋ pH 12.7 refolding and unfolding (▽), and S_∞ from pH 7 → 12.7 refolding (□) reactions. Small solid circles through S_o data in both panels are fits to the empirical relation $S_0 = a + b \exp(cx)$, where *a*, *b*, *c* are constants, and *x* is the concentration of GdnHCl. The solid lines through S_∞ data reproduce equilibrium stabilities under the final refolding−unfolding conditions.

Denaturant Dependence of Burst Folding Signals. For all refolding reactions studied, a substantial fraction of the total expected fluorescence is lost in a burst phase that is completed within the dead-time of the stopped-flow. The burst phase analysis is based on the idea that GdnHCl dependence of the baseline signal (or $t \rightarrow \infty$ signal) of the burst kinetic phase, extracted by extrapolating the observed refolding curve to zero time (S_0), produces an unfolding transition curve of the burst folding intermediate (*29*). It provides an approach to view the sub-millisecond regime when microsecond events have not been resolved in real-time. Unfortunately, the procedure suffers from practical limitations of obtaining relatively accurate burst relaxation data. Nevertheless, Figure 4a presents this analysis for pH 7 → 7 and pH 12.7 → 7 refolding reactions. In neither case do the GdnHCl dependences of S_0 values indicate, within error, a distinct denaturant-induced phase transition. One may choose to interpret such a curve as a sigmoidal plot which is missing the pretransition, and thus the shape of the curve could simply reflect marginal stability of an intermediate. But, as discussed in detail in the preceding article in this issue (*26*), the curves rather appear to simulate the GdnHCl dependence of fluorescence of the unfolded cyt *c*. In contrast, the GdnHCl dependence of $t = \infty$ signals of the observed refolding and unfolding traces (S_∞) produce a cooperative transition closely similar to the equilibrium unfolding curve for neutral ferrocyt *c* (Figure 2a). In Figure 4b, the same analysis is presented for pH 7 → 12.7 and

pH 12.7 → 12.7 refolding reactions. Again, the GdnHCl dependences of S_0 signals are atypical of a cooperative transition, unlike the S_∞ signals whose denaturant titration reproduces the equilibrium unfolding transition of alkaline ferrocyt *c* (Figure 2a). Thus, burst phase products are unlikely to contain structures. This view is justified by experimental data and arguments given in the previous article.

Imprinted Burst Product. The closeness of S_0 distributions shown for pH 7 → 7 and pH 12.7 → 7, and for pH 7 → 12.7 and pH 12.7 → 12.7 refolding reactions (Figure 4a,b) provides a fundamental insight to the response of the unfolded chains when they are allowed to refold. The unfolded states of ferrocyt *c* at neutral and alkaline pH are unlikely to be similar at least structurally due mainly to differences in ionization and chain solvation. No matter how different they are in terms of chain configuration, chain solvation, or even stability, their fluorescence signals on being driven to refold under a given final solvent condition are nearly identical, suggesting that the earliest relaxation or reconfiguration of the chains (U → U′) must be the same and is independent of the initial equilibrium unfolded state (U).

The GdnHCl dependences of S_∞ values obtained from pH 7 → 7 and pH 12.7 → 7 refolding reactions are same within experimental error (Figure 4a), indicating that the refolded native proteins under a given final condition are structurally identical irrespective of the initial unfolded state. The same argument holds for the S_∞ data shown for pH 7 → 12.7 and pH 12.7 → 12.7 refolding reactions (Figure 4b). These results provide a basis for phenomenological description of protein folding kinetics.

DISCUSSION

Folding Kinetics: Disagreements with Theoretically Based Ideas. From the landscape perspective, one might imagine a rather smooth funnel for the folding of ferrocytochrome *c* where kinetics are fast and essentially two-state, involving no significant kinetic traps. But the simple kinetic analysis of cytochrome systems presents an instructive case in which experimental results do not meet with some of the basic tenets of the landscape paradigm. First, notwithstanding the disparity of ~15 kcal mol^{-1} in global thermodynamic stability, the refolding speeds of neutral and alkaline ferrocyt *c* to a given final pH are not strongly different (Table 1), and this is so even though ferrocyt *c* folds in a two-state manner. This implies poor dependence of folding speed on global thermodynamic driving force, in contrast with the landscape view that holds that folding is rate-limited by the size, slope, and depth of the folding funnel (*12*, *30*, *31*). Second, for both neutral and alkaline ferrocyt *c*, regardless of the final refolding pH, the activation energy barrier is in the range 7−8 kcal mol^{-1}. This is a sizable barrier, and it has contributions from both energetic and entropic components. In contrast, theory and simulation results for general downhill folding entails no apparent barrier (*15*), or perhaps a tiny barrier equal to a few k_BT (*11*, *32*). A transition-state barrier or a bottleneck in the funneling process can appear when the compensation of enthalpic and entropic components is mismatched (*18*). More specifically, smooth-funneling witnesses no apparent barrier or no specific bottleneck conformation. The folding rate is intrinsically limited by the steepness and the size of the funnel (*12*). Third, for all refolding experiments conducted here, the α-value for refolding is less than 0.3, meaning that less than one-third of the surface that is buried in the native state gets buried in the transition state. This resemblance of the transition state to the unfolded state is inconsistent with the landscape approach that suggests that the folding transition ensemble appears at a time when a substantial fraction of native contacts are already formed (*11*, *14*, *32*, *33*).

These conflicts between experiments and theory have been noted in another study of three variants of ferrocyt *c* under physiological pH, 10 °C (*25*). The "RYGB model" of cyt *c* advanced by Englander and co-workers from extensive native-state kinetic hydrogen exchange incorporates the basic elements of the pathway concept of protein folding (*20*−*23*). Disagreements between the two folding paradigms have been noted for other two-state proteins as well (*24*). Taken together, the observations presented fit precisely into the picture of classical kinetic models with folding rates largely governed by the energy gap between the unfolded state and the transition state.

The Classical Perspective. The results afford a phenomenological description of folding events.

(*i*) *Kinetically Constrained Ultrafast Relaxation.* As soon as a refolding condition is created the unfolded chains (U) initially at low-energy equilibrium states are driven instantaneously to new higher energy level(s) (*33*). The excited chains, now in nonequilibrium states, respond to the new solvent condition where only a few, if any, denaturant molecules can affect the nascent polypeptides (U′). The exact nature of this ultrafast relaxation is not clear. As discussed in the accompanying article in this issue, it may involve collapse or chain contraction, desolvation, and/or redistribution of backbone dihedral $\varphi-\psi$ angles (*10*, *25*, *34*, *35*). It is missed out in millisecond stopped-flow measurements and is termed burst folding phase (Figure 4). The burst relaxation may escape experimental detection if the probe employed is silent to the U → U′ relaxation (*36*).

Figure 5 schematizes folding of two configurationally different unfolded states of the same amino acid sequence to a given refolding condition, say, pH 7 → 7 and pH 12.7 → 7 or pH 7 → 12.7 and pH 12.7 → 12.7 refolding reactions. Instantaneous with the refolding jump is the deformation of initial unfolded energy levels. Under the same refolding condition, the "zero-time" nonequilibrium states of neutral and alkaline ferrocyt *c*, which are not yet relaxed, may or may not be different. In any case, at the end of the ensuing relaxations the nascent states (U′) derived from neutral-unfolded and alkali-unfolded chains (U) are identical and energetically degenerate, as though a coherence has been established. This follows from near-concurrence of denaturant distributions of burst signals for pH 7 → 7 and pH 12.7 → 7, and the pH 7 → 12.7 and pH 12.7 → 12.7 refolding reactions (Figure 4). Implicit to the model is the deterministic nature of the U → U′ process. No matter how different structurally or configurationally are the initial unfolded states, it is the amino acid sequence that determines the nature of the relaxation, and the configuration and/or redistribution of dihedral angles in U′. This is a kinetically constrained process.

ΔG°_D values determined from equilibrium and kinetic experiments within a given pH (Table 1) appear to indicate

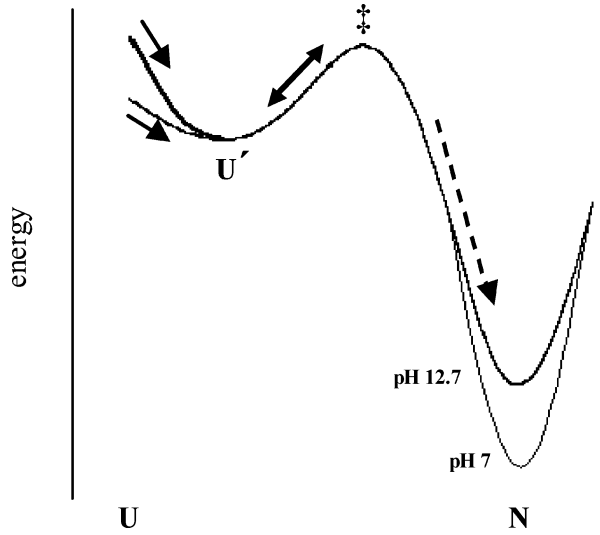

FIGURE 5: Schematic of the classical folding profile (U → U′ → ‡ → N). High-energy chains produced instantaneously with a refolding jump relax to the nascent state, U′, where they are energetically degenerate. A long search for an appropriate set of tertiary interactions that can support a nativelike chain topology ensues. The transition state is achieved when the correct combination of interactions develops. Folding then is rapid and energetically downhill, and is not strongly dependent on the slopes and depths of energy surfaces.

energetic similitude of U and U′ states. This follows from the result that aqueous stability of ferrocyt *c*, at a given pH, measured from equilibrium experiment appears indifferent to that estimated from kinetic experiments. Equilibrium data provide ΔG_D° for the two-state U ⇌ N reaction, whereas ΔG_D° calculated by using the rate constants reflects the energy difference between U′ and N, both under final refolding condition, since in millisecond kinetic experiments all information about the energetics of the initial U state is lost in the dead-time of mixing. The two U states may still differ in energy to some extent, but such differences are masked by error in data.

(*ii*) *Transition-State Topology Search and Barrier Crossing.* Because the U → U′ is a sub-millisecond relaxation and the experimentally observed folding time falls in the millisecond to seconds range, it is the U′ → N transition that sets the folding time. Further, for two-state fast-folding proteins such as ferrocyt *c* (*8*, *25*, *26*) and Csp B (*4*), where post-barrier kinetic intermediates do not accumulate, folding from the transition state to the native state will be rapid and barrier-free. These considerations imply that almost the entire length of the observed folding time is the time needed for the U′ state to find a supportive transition state. It consumes time because of the search-find nature of the process (*10*, *21*, *24*, *25*). It is thermodynamically constrained because a stable transition state that can support forward folding is to be found. The search continues until a relatively low-energy transition state stabilized by a few correctly formed nativelike tertiary contacts is achieved. This is the essence of the topology search model (*10*, *24*, *25*, *37*) that draws support from observations that folding rates and mechanisms often appear to be largely determined by the native-state topology or contact order (*38*−*40*). Nativelike chain topology stipulates certain long-range interactions, not local contacts as viewed by theory (*33*, *41*). In addition, being supported by only a few tertiary contacts the transition state must be dynamic and less organized, and therefore less nativelike, consistent with $\alpha < 0.3$ (Table 1). Even though the alkaline and neutral forms of ferrocyt *c* are somewhat different structurally, the minimal native-state contacts required in the transition state are probably unchanged, presumably because these portions of the native state are unchanged in the alkaline form of the protein. Finally, because the topology search is an unsystematic process, the possibility of error commitment is not excluded. A wrong transition barrier of low energy should lead to an off-pathway species, strong experimental evidence of which is beginning to emerge (unpublished result).

(iii) *Post-Barrier Folding.* Achieving the transition state is analogous to the assumption of the transition state theory that systems that have surmounted the col in the direction of products do not turn back. Folding is then rapid, especially in two-state cases such as ferrocyt *c* where post-barrier kinetic intermediates are so short-lived that they do not accumulate (*42*, *43*). In the absence of intermediates, there is no post-transition barrier, and therefore folding is simply downhill.

Results obtained with other test tube variants of cyt *c*, 10 °C (*10*, *25*), also lend support to this mechanistic description. Folding of many small proteins is expected to fit into this depiction. More empirical corroborations should be seen in times to come.

ACKNOWLEDGMENT

Authors are grateful to the anonymous reviewers for their insightful comments. Thanks are due to Drs. Bhadresh Rami and Jayant Udgaonkar for stimulating discussions and suggestions. D.K.R. is supported by the Council of Scientific & Industrial Research. A.K.B. is the recipient of a Swarnajayanti Fellowship from the Department of Science & Technology, Government of India.

REFERENCES

1. Matthews, C. R. (1993) Pathways of protein folding, *Annu. Rev. Biochem. 62*, 653−683.
2. Ptitsyn, O. B. (1995) Molten globule and protein folding, *Adv. Protein Chem. 47*, 83−229.
3. Huang, G. S., and Oas, T. G. (1995) Submillisecond folding of monomeric lambda repressor, *Proc. Natl. Acad. Sci. U.S.A. 92*, 6878−6882.
4. Schindler, T., Herrler, M., Marahiel, M. A., and Schmid, F. X. (1995) Extremely rapid protein folding in the absence of intermediates, *Nat. Struct. Biol. 2*, 663−673.
5. Perl, D., Welker, C., Schindler, T., Schröder, K., Marahiel, M. A., Jaenicke, R., and Schmid, F. X. (1998) Conservation of rapid two-state folding in mesophilic, thermophilic and hyperthermophilic cold shock proteins, *Nat. Struct. Biol. 5*, 229−235.
6. Wildegger, G., Liemann, S., and Glockshuber, R. (1999) Extremely rapid folding of the c-terminal domain of the prion protein without kinetic intermediates, *Nat. Struct. Biol. 6*, 550−553.
7. Sato, S., Luisi, D. L., and Raleigh, D. P. (2000) pH jump studies of the folding of the multidomain ribosomal protein L9: the structural organization of the N-terminal domain does not affect the anomalously slow folding of the c-terminal domain, *Biochemistry 39*, 4955−4962.
8. Bhuyan, A. K., and Udgaonkar, J. B. (2001) Folding of horse cytochrome *c* in the reduced state, *J. Mol. Biol. 312*, 1135−1160.
9. Sosnick, T. R., Mayne, L., Hiller, R., and Englander, S. W. (1994) The barriers in protein folding, *Nat. Struct. Biol. 1*, 149−156.
10. Sosnick, T. R., Mayne, L., and Englander, S. W. (1996) Molecular collapse: The rate-limiting step in two-state cytochrome *c* folding, *Proteins 24*, 413−426.

11. Onuchic, J. N., Wolynes, P. G., Luthey-Schulten, Z., and Socci, N. D. (1995) Toward an outline of the topography of a realistic protein-folding funnel, *Proc. Natl. Acad. Sci. U.S.A. 92*, 3626−3630.
12. Dill, K. A., and Chan, H. S. (1997) From Levinthal to pathways to funnels, *Nat. Struct. Biol. 4*, 10−19.
13. Onuchic, J. N., Luthey-Schulten, Z., and Wolynes, P. G. (1997) Theory of protein folding: the energy landscape perspective, *Annu. Rev. Phys. Chem. 48*, 545−600.
14. Socci, N. D., Onuchic, J. N., and Wolynes, P. G. (1998) Protein folding mechanisms and the multidimensional folding funnel, *Proteins 32*, 136−158.
15. Schonbrun, J., and Dill, K. A. (2003) Fast protein folding kinetics, *Proc. Natl. Acad. Sci. U.S.A. 100*, 12678−12682.
16. Onuchic, J. N., and Wolynes, P. G. (2004) Theory of protein folding, *Curr. Opin. Struct. Biol. 14*, 70−75.
17. Baldwin, R. L. (1995) The nature of protein folding pathways: the classical versus the new view, *J. Biomol. NMR 5*, 103−109.
18. Bryngelson, J. D., Onuchic, J. N., Socci, N. D., and Wolynes, P. G. (1995) Funnels, pathways and the energy landscape of protein folding: a synthesis, *Proteins 21*, 167−195.
19. Onuchic, J. N., Socci, N. D., Luthey-Schulten, Z., and Wolynes, P. G. (1996) Protein folding funnels: the nature of the transition state ensemble, *Folding Des. 1*, 441−450.
20. Bai, Y., Sosnick, T. R., Mayne, L., and Englander, S. W. (1995) Protein folding intermediates: native state hydrogen exchange, *Science 269*, 192−197.
21. Rumbley, J., Hoang, L., Mayne, L., and Englander, S. W. (2001) An amino acid code for protein folding, *Proc. Natl. Acad. Sci. U.S.A. 98*, 105−112.
22. Hoang, L., Bédard, S., Krishna, M. M. G., Lin, Y., and Englander, S. W. (2002) Cytochrome *c* folding pathway: kinetic native-state hydrogen exchange, *Proc. Natl. Acad. Sci. U.S.A. 99*, 12173−12178.
23. Krishna, M. M. G., Lin, Y., Rumbley, J. N., and Englander, S. W. (2003) Cooperative omega loops in cytochrome *c*: role in folding and function, *J. Mol. Biol. 331*, 29−36.
24. Makarov, D. E., and Plaxco, K. W. (2003) The topomer search model: a simple, quantitative theory of two-state protein folding kinetics, *Protein Sci. 12*, 17−26.
25. Prabhu, N. P., Kumar, R., and Bhuyan, A. K. (2004) Folding barrier in horse cytochrome *c*: support for a classical folding pathway, *J. Mol. Biol. 337*, 195−208.
26. Kumar, R., and Bhuyan, A. K. (2005) Two-state folding of horse ferrocytochrome *c*: analyses of linear free energy relationship, chevron curvature, and stopped-flow burst relaxation kinetics, *Biochemistry 44*, xxx−xxx.
27. Silow, M., and Oliveberg, M. (1997) High-energy channeling in protein folding, *Biochemistry*, *36*, 7633−7637.
28. Krieger, F., Fierz, B., Bieri, O., Drewello, M., and Kiefhaber, T. (2003) Dynamics of unfolded polypeptide chains as model for the earliest steps in protein folding, *J. Mol. Biol*. *332*, 265−274.
29. Ikeguchi, M., Kuwajima, K., Mitani, M., and Sugai, S. (1986) Evidence for identity between the equilibrium unfolding intermediate and a transient folding intermediate: a comparative study of the folding reactions of α-lactalbumin and lysozyme, *Biochemistry 25*, 6965−6972.
30. Shakhnovich, E. I., and Gutin, A. M. (1993) Engineering of stable and fast-folding sequences of model proteins, *Proc. Natl. Acad. Sci. U.S.A. 90*, 7195−7199.
31. Socci, N. D., and Onuchic, J. N. (1994) Folding kinetics of protein-like heteropolymer, *J. Chem. Phys. 101*, 1519−1528.
32. Wolynes, P. G., Onuchic, J. N., and Thirumalai, D. (1995) Navigating the folding routes, *Science 267*, 1619−1620.
33. Shakhnovich, E. I. (1997) Theoretical studies of protein-folding thermodynamics and kinetics, *Curr. Opin. Struct. Biol. 7*, 29−40.
34. Sosnick, T. R., Shtilerman, M. D., Mayne, L., and Englander, S. W. (1997) Ultrafast signals in protein folding and the polypeptide contracted state, *Proc. Natl. Acad. Sci. USA*, *94*, 8545−8550.
35. Jacob, J., Krantz, B., Dothager, R. S., Thiyagarajan, P., and Sosnick, T. R. (2004) Early collapse is not an obligate step in protein folding, *J. Mol. Biol. 338*, 369−382.
36. Magg, C., and Schmid, F. X. (2004) Rapid collapse precedes the fast two-state folding of the cold shock protein, *J. Mol. Biol*. *335*, 1309−1323.
37. Plaxco, K. W., Simons, K. T., and Baker, D. (1998) Contact order, transition state placement and the refolding rates of single domain proteins, *J. Mol. Biol. 277*, 985−994.
38. Baker, D. (2000) A surprising simplicity to protein folding, *Nature 405*, 39−42.
39. Plaxco, K. W., Simons, K. T., Ruczinski, I., and Baker, D. (2000) Topology, stability, sequence, and length: defining the determinants of two-state protein folding kinetics, *Biochemistry 39*, 1177−11183.
40. Bai, Y., Zhou, H., and Zhou, Y. (2004) Critical nucleation size in the folding of small apparently two-state proteins, *Protein Sci. 13*, 1173−1181.
41. Abkevich, A. I., Gutin, A. M., and Shakhnovich, E. I. (1995) Impact of local and nonlocal interactions on thermodynamics and kinetics of protein folding, *J. Mol. Biol. 252*, 460−471.
42. Bhuyan, A. K., and Udgaonkar, J. B. (1998) Stopped-flow NMR measurement of hydrogen exchange rates in reduced horse cytochrome *c* under strongly destabilizing conditions, *Proteins 32*, 241−247.
43. Xu, Y., Mayne, L. C., and Englander, S. W. (1998) Evidence for an unfolding and refolding pathway in cytochrome *c*, *Nat. Struct. Biol*. *5*, 774−778.

BI047897N